Lasers in Surgery and Medicine 18:22–33 (1996)

In Vitro Studies and Computer Simulations to Assess the Use of a Diode Laser (850 nm) for Laser-Induced Thermotherapy (LITT)

Viravuth Prapavat, MS, André Roggan, MS, Jakob Walter, MD, Jürgen Beuthan, PhD, Ulrich Klingbeil, PhD, and Gerhard Müller, PhD

Institut für Medizinische/Technische Physik und Lasermedizin des Universitätsklinikum Benjamin Franklin (V.P., J.B., G.M.), and Institut für Veterinär-Pathologie (J.W.), Freie Universität, and Laser-Medizin-Zentrum gGmbH (A.R., G.M.), 12207 Berlin, Germany, and MetaSystems, Belmont, Massachusetts 02178 (U.K.)

Background and Objective: **This study investigated the feasibility of 850 nm diode laser-induced thermotherapy (LITT), a new procedure providing local hyperthermia and photocoagulation, a minimally invasive treatment of tumors, and other disorders such as benign prostate hyperplasia.**
Study Design/Material and Methods: **An improved fiber optic diffuser inserted through a catheter was used to irradiate prostate, liver, and kidney tissue in-vitro. Experimental results were compared with predictions from mathematical simulations based on measured optical tissue parameters.**
Results: **After 10 minutes of irradiation with 2–4.6 W CW laser power, sizable coagulation diameters had been achieved. In prostate and kidney tissue, temperature rises and coagulation diameters after laser irradiation were found to be smaller than in liver tissue. Those tissues also had a higher threshold for carbonization, thus reducing the risk of damage to the delivery system.**
Conclusion: **The data suggest that a low power diode laser can be recommended for use in LITT to treat prostate and kidney tissue.** © 1996 Wiley-Liss, Inc.

Key words: diode laser, interstitial hyperthermia, laser applicator, laser induced thermotherapy, optical tissue parameters

INTRODUCTION

Laser-induced thermotherapy (LITT) is a new procedure for local hyperthermia and photocoagulation allowing minimally invasive treatment of tumors and other disorders such as benign prostate hyperplasia [1–7]. The treatment effect, generally long-term tissue damage, is based on a variety of thermal laser-tissue interactions characterized in Table 1. Absolute temperature and exposure duration are the most important parameters used to predict tissue damage (Fig. 1) [8]. The threshold for irreversible tissue damage also depends on the type of tissue and its metabolism, and it carries significant statistical variations, which add complexity to the simplified model presented in Figure 1.

The Nd:YAG laser has become the standard tool for LITT. The advent of fiber-coupled, high-power semiconductor laser systems in the power range up to 25 W opens an interesting prospective for new LITT devices, which may offer some advantages over current devices: (1) Diode lasers for medical applications can be made relatively compact, light weight, and less expensive, and (2) output power levels of only a few watts can be precisely controlled and maintained constant.

The present study evaluated the potential

Accepted for publication August 21, 1994.

Address reprint requests to Ulrich Klingbeil, 76 Fairview Avenue, Belmont, MA 02178.

© 1996 Wiley-Liss, Inc.

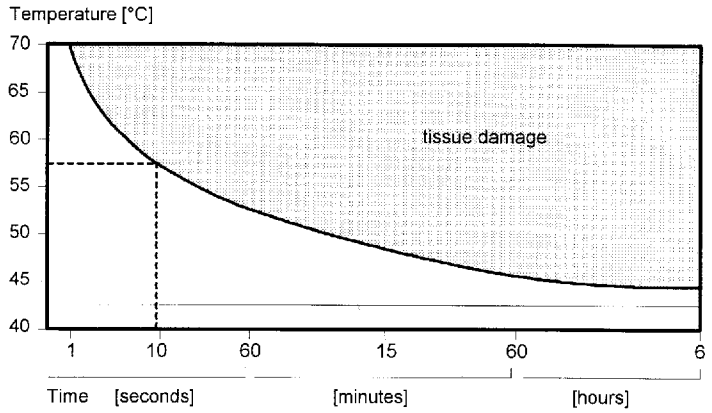

Fig. 1. Threshold for tissue damage as a function of temperature and exposure time [8].

Table 1. Thermal Laser Tissue Interactions

Photochemical Effects		
Photoinduction	Biostimulation	
Photoactivation of Drug	POD	
Photoradiation		
Photochemotherapy	Photodynamic Therapy (PDT)	
	Black Light Therapy (PUVA)	
Photoresonance		
Photothermal Effects		
Photothermolysis	Thermal-Dynamic Effects, microscale overheating	
Photohyperthermia[a]	37°–43°C	no irreversible damage of normal tissue
	45°–60°C	loosening of membranes (edema), tissue welding, denaturation of enzymes
Photocoagulation[a]	60°–100°C	coagulation, necrosis
Photocarbonization	100°–300°C	drying out, vaporization of water, carbonization
Photovaporization	>300°C	pyrolysis, vaporization of solid tissue matrix
Photoionization or Photodecomposition		
Photoablation	fast thermal explosion (e.g. Angioplasty)	
Photodisruption	optical breakdown, mechanical shockwave	
Photofragmentation	(e.g. Lithotripsy)	

[a]Represents LITT.

clinical usefulness of a 5 W diode laser (850 nm) for LITT in prostate, liver, and kidney tissue. The study attempted to answer the following questions: Which technical specifications apply for the laser and the laser delivery system? Is the use of a diode laser for LITT, in principle, advantageous? Can a mathematical simulation with measured optical tissue parameters predict a scenario for the beneficial use of the diode laser for LITT? Do simulations agree with experimental in vitro measurements?

MATERIALS AND METHODS

In Vitro Experiments

The experiments for laser-induced thermotherapy were carried out with a prototype fiber-coupled GaAlAs semiconductor laser DL-4000 (Candela Laser Corp., Wayland, MA). The system delivered a maximum CW output power of 5 W at a wavelength of 850 nm. The power level and exposure duration were preset and controlled by an internal microprocessor.

To deliver the laser energy to the tissue, a fiber optic applicator for thermotherapy was refined and tested. The applicator was inserted into a distally closed catheter made of thermoplastic fluoropolymer (B.Braun, Melsungen) before it was introduced into the tissue. This prevented contamination of the applicator, increased its overall outside surface, and provided protection from mechanical stress. The system provided a homogeneous photon distribution in tissue and was attached to the laser by SMA connector. Fig-

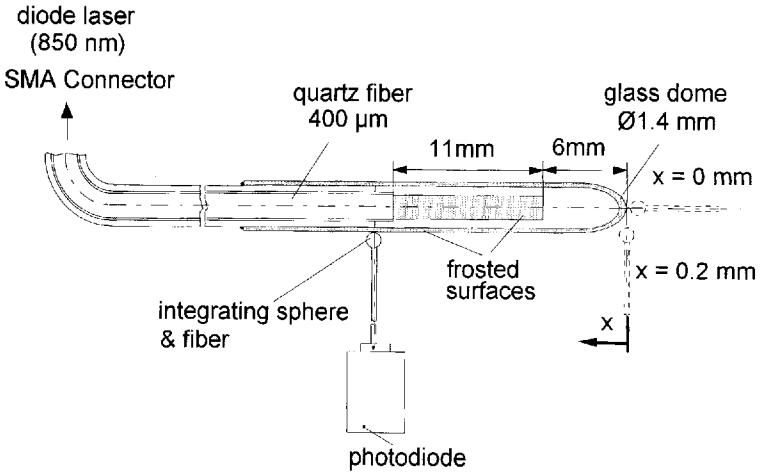

Fig. 2. Schematics of LITT applicator and setup to measure near-field radiation.

ure 2 shows the setup used to measure the near field intensity distribution.

Two NiCr-Ni thermocouples (Philips, Type 2ABAc05) interfaced to an analyzing recorder (Yokogawa, Model 3665E) were used to measure the temperature at regular intervals throughout the experiments. Self-absorption of the thermocouples, which could cause erroneous values, was assumed to be negligible since their distances to the applicator were larger than the penetration depth of the laser light [9].

A rigid mechanical fixture was used to mount the catheter with introduced fiber optic diffuser and achieve reproducible positioning and alignment with the temperature sensors (Fig. 3). The fixture had equidistant holes, each 5 mm apart, for the catheter and the thermocouples normally placed at opposite sides of the applicator, 5 mm and 10 mm away from the applicator axis.

The laser tissue effect of the diode laser radiation was evaluated for the following tissues: prostate (canine), liver (porcine), and kidney (porcine). Tissue samples were used at room temperatures (20°C), some freshly harvested, ex-vivo, or after short-term refrigeration at −22°C. The irradiated tissues were dissected shortly after treatment and cut with a cryotome. The tissues were stained by the Trichrome-Goldner method since it provided a better determination of coagulated areas by observation of the macroscopic tissue color than the usually applied HE-staining method [10].

In liver and kidney tissue, the catheter was directly introduced into the tissue. For prostate tissue, it was introduced transurethrally since the relatively small size of the isolated glands did not allow direct placement into one of the lobes.

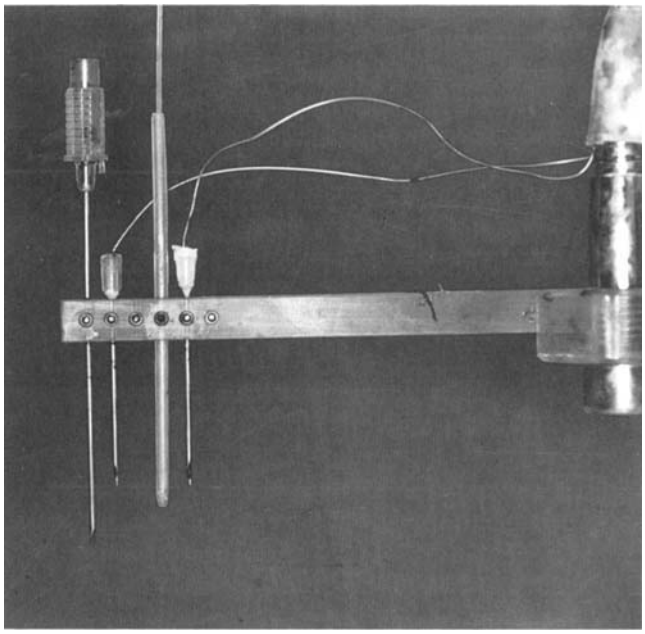

Fig. 3. Mechanical mount with applicator in catheter and thermocouples.

Measurement of Optical and Thermal Tissue Parameters

To determine optical tissue parameters, the optical setup shown in Figure 4 was used [11]. A thin tissue sample placed between two integrating spheres (Labsphere, North Sutton, NH) was illuminated by collimated light of 850 nm. The tissue was homogenized in a mortar at 77K and filled into quartz cuvettes of calibrated thickness,

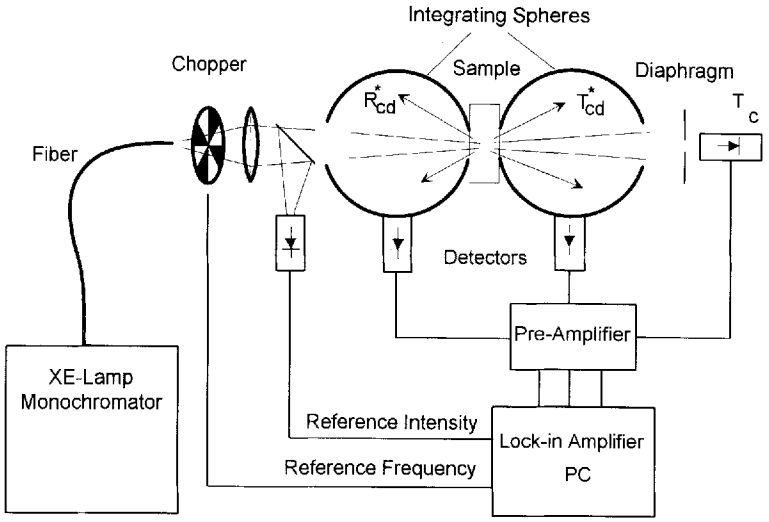

Fig. 4. Double integrating sphere setup to measure optical tissue parameters.

ranging from 100 μm to 500 μm. This procedure provided cell clusters of ~50–500 μm in diameter, which were assumed to have the same optical properties as the original tissue [12].

Four detectors read the diffuse backscattering, the diffuse transmission, the collimated transmission, and the reference intensity. These values were used to calculate the optical tissue parameters: absorption coefficient μ_a [mm^{-1}], scattering coefficient μ_s [mm^{-1}], and the anisotropy factor g. To calculate the effective penetration depth δ a reduced scattering coefficient $\mu_s' = \mu_s(1 - g)$ was introduced in the diffusion approximation [13] yielding:

$$\delta = \frac{1}{\sqrt{3\mu_a(\mu_a + \mu_s(1 - g))}}.$$

A program based on inverse Monte Carlo calculations was developed to calculate the optical tissue parameters, taking into account sideward losses of photons as well as specular reflections at boundaries. The parameters were fitted by the gradient method [11]. For the determination of the g factor, we assumed that scattering in tissue may be described with the Henyey-Greenstein phase function.

The thermal tissue parameters heat conduction λ, heat capacity c_p, and density ρ were calculated based on the tissue water content by using the formulas of Takata [14,15]. For liver tissue, the water content (by weight) was assumed to be 68%, and for kidney, 83%. The water content of prostate tissue was measured from two fresh human prostate samples to be 82 ± 0.5%. As these samples exhibited substantial hyperplasia, the value for the water content was corrected to 80 ± 3% to include the more typical prostates which were used for the in vitro experiments.

Simulation

A mathematical model was developed to predict the photon distribution inside the tissue, the transformation of absorbed radiation into thermal energy, the influence of heat conduction, blood perfusion, and the resulting tissue reaction [16]. The simulation required knowledge of the optical and thermal parameters in the native as well as in the coagulated state.

The radiation flux is given by the photon transport equation, which was solved analytically by applying the diffusion approximation with $\mu_a << \mu_s'$, a valid assumption at 850 nm [12]. The change of optical tissue properties $x = \{\mu_a, \mu_s, g\}$ during the process of photocoagulation was approximated through an interpolation between the optical parameters for the native x_n and the coagulated tissue x_c weighted by the coagulation radius r_c: $x_a = x_n + (x_c - x_n)(1 - \exp(-r_c/\delta))$.

The local temperature rise within each small increment of time is a function of the calculated photon flux and heat conduction. It can be expressed as a partial differential equation of thermal diffusion (bio heat equation) [17]. The equation was solved for spherical coordinates using the method of Finite Differences [18] assuming the applicator had a spherical geometry and the

same surface area as the applicator used in the experiments.

The tissue damage was calculated numerically by the Arrhenius rate equation [15] using the tissue specific rate coefficient A = $9.4 \times 10^{104} s^{-1}$, the activation energy E = 6.68×10^5 J/mol and the universal gas constant R = 8.31 J/(mol·K) [15,20]:

$$\Omega(T,t) = A\int_0^t \exp\left(-\frac{E}{RT(t)}\right) dt. \qquad (1)$$

The damage integral Ω describes the probability for protein denaturation as a function of temperature T and time t: Ω = 1 corresponds to a 63% denaturation. A value of Ω = 0.53 was used for the threshold of irreversible tissue damage according to the studies of Henrique [8]. The resulting damage radius delineates the zone of irreversible damage.

The radius of coagulation was introduced to describe the extent of acute tissue changes, which should be easier to visualize in experiments. To determine the radius of coagulation and the effect of the progressing coagulation on the optical tissue properties each volume element (voxel) was marked "coagulated" as soon as the threshold temperature of 60°C was reached. A threshold of 60°C was chosen because at this temperature irreversible tissue damage (Ω = 0.53) occurs after only 3 seconds and the delay is negligible compared to the typical exposure time of 10 minutes (Fig. 1).

To allow for the simulation of in vivo conditions, the influence of blood perfusion was included in the model. A loss term was introduced for those voxels that were not marked coagulated. Coagulated voxels were assumed to have no perfusion due to shrinkage of capillary vessels. Since no published perfusion rates for human prostate tissue were found in the literature calculations were performed with two estimated perfusion rate values of 0.2 and 0.4 ml/(g·min). For liver tissue, rates of 0.5 and 1.0 ml/(g·min) and for kidney tissue of 2 and 4 ml/(g·min) were used [19].

The simulation of the temperature distribution was calculated on a 486/66 PC at intervals of 0.033 s and a spatial resolution of 0.1 mm. The program needed ~4.5 minutes to simulate the temperature distribution throughout an exposure time of 15 minutes. The temperature was presented graphically after each time interval yielding a comprehensive display of the temperature response. The calculated coagulation radius (T> 60°C), the damage radius (Ω> 0.53), and the radius of vaporization (T> 100°C) were also included in the graph. In addition, the program could calculate the time required to reach a preset damage diameter that allows to recommend exposure durations for irradiation planning.

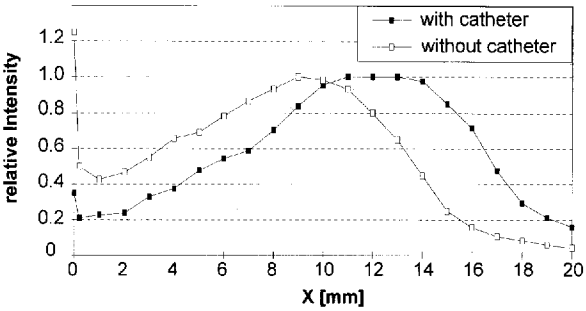

Fig. 5. Near-field radiation pattern of LITT applicator. 0-position refers to applicator/catheter tip.

The simulation does not predict carbonization because its strong dependence on cell structure and tissue vaporization is difficult to quantify.

RESULTS

Applicator

The final design of the fiber optic delivery system after refinement and testing throughout this study specifies a plastic clad silica fiber (PCS, Ø = 400 μm) where 11 mm of the cladding and the coating at the distal end were removed and the remaining core was frosted by chemical etching. In addition, the fiber tip was enclosed in a glass dome of 1.4 mm outer diameter with etching on its interior surface to reduce the remaining forward directed component of the radiation. The fiber assembly was inserted in a thermoplastic fluoropolymer Hostaflon (Hoechst) catheter with an outer diameter of 2.3 mm. Figure 5 illustrates the near field radiation characteristic of the applicator with and without catheter.

Optical Tissue Parameters

The optical parameters derived from the measurements for prostate, liver and kidney tissue at a wavelength of 850 nm are listed in Table 2.

The reproducibility of the measurements and calculations of optical tissue properties was analyzed to assess the influence of the preparation process, the experimental setup, and the sta-

TABLE 2. Optical Tissue Parameters Derived From Measurement: Absorption Coefficient (μ_a), Scattering Coefficient (μ_s), Anisotropy Factor (g), Reduced Scattering Coefficient (μ_s'), and Penetration Depth (δ) for Prostate, Liver, and Kidney Tissue

	Prostate water content: 80%		Liver water content: 68%		Kidney water content: 83%	
850 nm	Native	Coagulated	Native	Coagulated	Native	Coagulated
μ_a [mm^{-1}]	0.055	0.065	0.12	0.13	0.11	0.12
μ_s [mm^{-1}]	12	26	10	42	7	32
g [mm^{-1}]	0.96	0.96	0.96	0.94	0.96	0.95
μ_s' [mm^{-1}]	0.48	1.04	0.4	2.52	0.28	1.6
δ [mm^{-1}]	3.4	2.2	2.3	1.0	2.8	1.3

tistical nature of the Monte Carlo simulation. Multiple measurements and calculations were carried out with one type of sample tissue (human tonsil) of one individual. The tissue was separated in 10 parts, each prepared and homogenized separately. The samples were measured at 633 nm and the optical parameters were calculated using the inverse Monte Carlo simulation. The variations for all parameters were within ±2.5%.

The interindividual variability of optical parameters of the same type of tissue is much larger than the intrasample variability. It depends on differences in tissue density, blood content, water content, etc. Our experience with healthy tissues indicated that the respective differences in optical parameters may be as high as 30% for the scattering and the absorption coefficient and up to 5% for the anisotropy factor. Tumor tissues may show even larger differences depending on the malignancy [21].

In Vitro Experiments

A sample of prostate tissue after treatment (4,6W; 20 min.) and preparation is shown in Figure 6. The staining (Trichrome-Goldner) outlines the coagulated region by a light red hue, whereas the native tissue shows a light green coloration.

For prostate tissue, the time-dependent temperature response was recorded for the power levels of 4 and 4.6 W (Fig. 7). Coagulation diameters of 10–17 mm were measured for power levels from 3 to 4.6 W and exposure times of 10–20 minutes (Table 3). The total energy applied ranged from 1,800 to 5,520 J. Carbonization was observed for power levels of 4W and above for exposure times of 15 minutes and above.

For liver tissue, the recorded temperature response is shown in Figure 8. Coagulation diameters of 9–19 mm were measured for power levels from 2 to 3 W and an exposure time of 10 minutes (Table 4). First, small areas of carbonization were

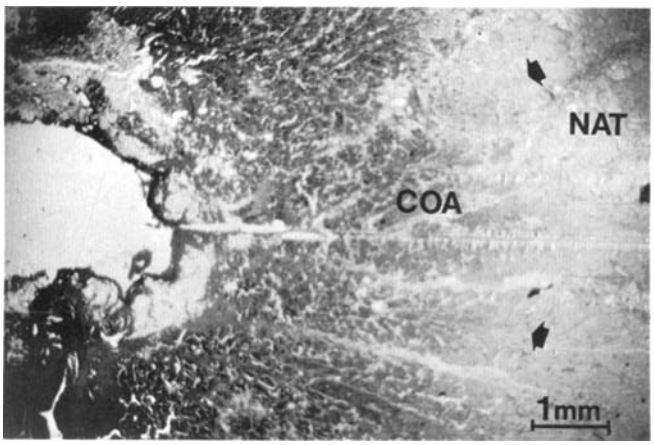

Fig. 6. Prostate tissue including urethra after treatment (4,6 W; 20 min.), preparation, and staining (Trichrome-Goldner) with 1 mm bar. Arrows outline the area of coagulation (COA).

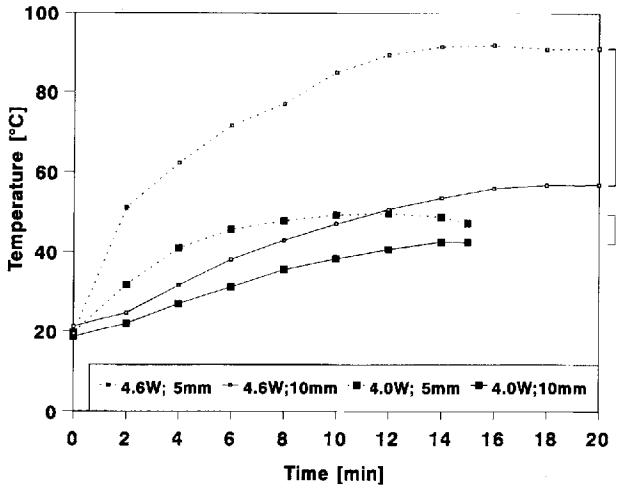

Fig. 7. Measured temperature response for LITT of prostate.

observed for power levels as low as 2.5 W, whereas at 3W and above a larger carbonization area was produced that led to a destruction of the applicator. The total energy applied ranged from 1,200 to 1,800 J.

TABLE 3. Measured and Calculated Coagulation (coag) and Damage (dam) Diameters for Prostate Tissue In Vitro

Prostate Laser power [W]	Coagulation and damage diameter [mm]								
	Exposure time: 10 min			Exposure time: 15 min			Exposure time: 20 min		
		Simulated			Simulated			Simulated	
	Measured	Coag.	Dam.	Measured	Coag.	Dam.	Measured	Coag.	Dam.
3.0	10	7.8	10.2	11	9.4	12.4	12	10.4	13.8
3.5	10	9.8	12.4		11.4	14.4	12	12.4	15.8
4.0	13	11.4[a]	13.8[a]	12[b]	13.0[a]	16.0[a]	14[b]	14.2[a]	17.6[a]
4.6	13	13.0[a]	15.4[a]		14.8[a]	17.8[a]	17[b]	16.0[a]	19.4[a]

[a]Temperatures over 100°C at the applicator.
[b]Carbonization.

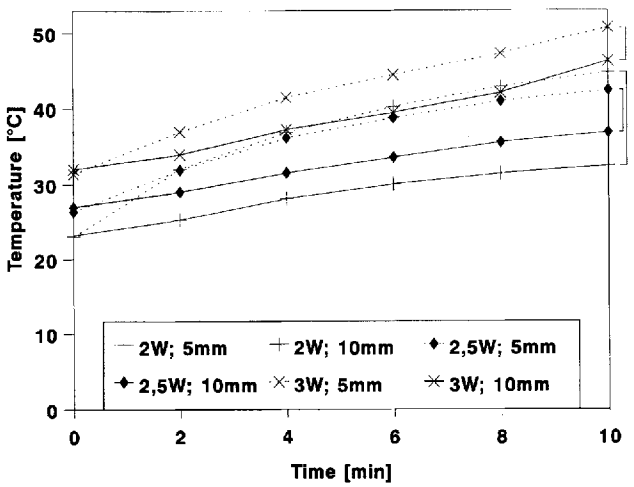

Fig. 8. Measured temperature response for LITT of liver.

For kidney tissue, the recorded temperature response is shown in Figure 9. Coagulation diameters of 5–11 mm were measured for power levels from 2 to 4 W and an exposure time of 10 minutes (Table 4). The threshold for carbonization at 10 minutes was >4 W.

The error in measuring the induced coagulation diameter is below ±1 mm assuming that in vitro conditions, especially the native water content and native tissue coloration remain constant.

The reproducibility of the temperature values depends on the uncertainty of placing the thermocouples. Despite the rigid mechanical fixtures, positioning errors may be as high as ±1 mm. Deviations in the axial positioning of the thermocouples relative to the applicator may cause additional errors. As a result, the variability of temperature values should be below 20% at 5 mm distance and within 10% at 10 mm distance due to smaller temperature gradients for larger distances from the applicator.

Simulations

A typical temperature response as predicted by the simulation is presented in Figure 10 for prostate tissue. The coagulation and damage diameters calculated from the optical tissue parameters are included in Tables 3 and 4 as a direct comparison to the in vitro measurements assuming an initial temperature of 20°C and no perfusion. Simulations in which the temperature exceeded 100°C at the applicator are highlighted in the tables.

The time required to create a potential damage diameter of 10, 15, or 20 mm in tissue at in vivo conditions was derived from the simulated temperature response as the time it would take to reach the damage threshold from an initial temperature of 36°C (Table 5). Computation was stopped after 1 hour if the preset damage diameter had not been reached (−).

DISCUSSION

Applicator

The first part of the study concentrated on the verification of a suggested delivery system for diode LITT. The characteristic near-field radiation pattern (Fig. 5), i.e., the photon distribution in the contact zone between the applicator surface and the tissue, was sufficiently homogeneous. There were no excessive local power spikes that would raise the risk of tissue carbonization due to particular high power densities.

Optical Tissue Parameters

The optical tissue parameters derived from the measurements showed significant differences between the tissues we investigated (Table 2). The absorption coefficient was twice as high for native liver or kidney as for native prostate, whereas prostate was more effective in scattering

TABLE 4. Measured and Calculated Coagulation (coag) and Damage (dam) Diameters for Prostate, Liver, and Kidney Tissue at 10-min Exposure Time In Vitro

Exposure time: 10 min Laser power [W]	Prostate			Liver			Kidney		
	Coagulation and damage diameter [mm]								
		Simulated			Simulated			Simulated	
	Measured	Coag.	Dam.	Measured	Coag.	Dam.	Measured	Coag.	Dam.
2.0			4.6	9	7.0	9.0	5		4.8
2.5		6.2	8.6	11[b]	9.0[a]	11.0[a]		7.0	9.0
3.0	10	7.8	10.2	19[b]	10.6[a]	12.8[a]	9	9.2	11.2
3.5	10	9.8	12.4		12.0[a]	14.0[a]		10.6[a]	12.8[a]
4.0	13	11.4[a]	13.8[a]		13.2[a]	15.4[a]	11	12.0[a]	14.0[a]
4.6	13	13.0[a]	15.4[a]		14.6[a]	16.6[a]		13.2[a]	15.4[a]

[a]Temperatures over 100°C at the applicator.
[b]Carbonization.

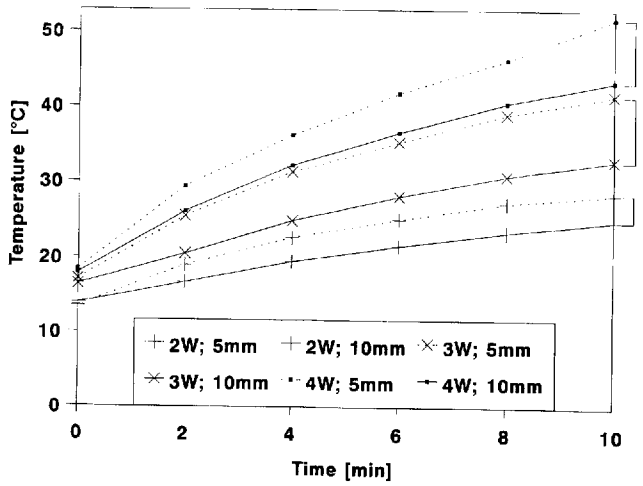

Fig. 9. Measured temperature response for LITT of kidney.

(μ_s') than liver and kidney. The penetration depth δ was between 2.3 mm and 3.4 mm for the native tissues. With coagulation, the penetration depth diminished notably and they were also more different for the different tissues (1.0–2.2 mm). The absorption coefficients hardly changed with coagulation; instead, the reduction of the penetration depth was a result of a two- to fourfold increase of the scattering coefficients.

In Vitro Experiments

The study of in vitro diode laser LITT at 850 nm demonstrated that sizable coagulation zones can be achieved without carbonization for prostate (13 mm), kidney (11 mm), and liver (9 mm) within a reasonable time of 10 minutes and power levels below 4 W (Table 4).

The temperature response characteristics were similar for prostate, kidney, and liver tissue. After 10 minutes of irradiation, the temperature response for all tissues with one exception (prostate, 4 W, 5 mm) showed a continuous temperature, rise suggesting that longer irradiation times would lead to higher temperatures (Figs. 7–9). After 10–15 minutes of higher level irradiation of prostate, the temperature had reached a steady state with no further temperature rise. The uncertainty of the temperature measurements and the experimental setup with isolated prostates limited the possibility to draw quantitative conclusions.

The analysis of the coagulation diameters in prostate indicated that an increase in exposure time of 100% from 10–20 minutes yielded only a 20% larger damage diameter (Table 3). An increase in laser power was much more effective in achieving larger coagulation diameters. Higher power levels, however, increased the risk of carbonization at long exposure times. This is particularly important for tissues with a small penetration depth (Table 4).

The threshold for carbonization in the in vitro measurements was considerably lower in liver tissue (2.5 W, 10 min.) than in prostate (>4.6 W, 10 min.) and kidney (>4.6 W, 10 min.). In liver the applied energy was deposited in a smaller volume than in prostate and kidney due to the lower penetration depth of the diode laser radiation. Additionally, due to the lower water content of liver, one would expect reduced heat conduction and a steeper temperature gradient resulting in the low threshold for carbonization. The risk for carbonization also increased with exposure time.

The study of diode LITT at 850 nm indicates some differences between the investigated tissues which may not be significant (Table 4). Coagulation diameters in liver were larger, whereas coagulation zones in kidney were slightly smaller than in prostate tissue. Data with carbonization

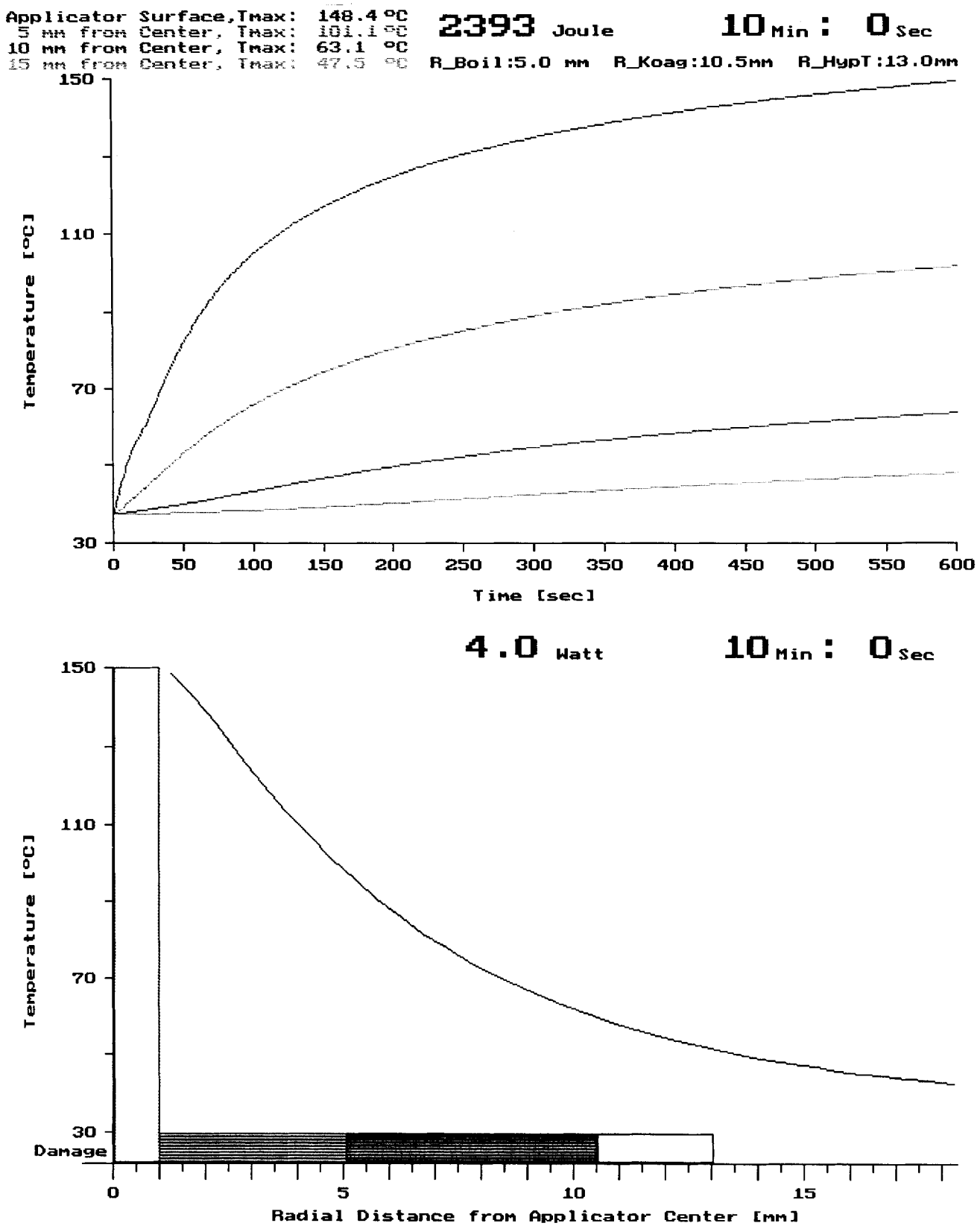

Fig. 10. Simulated temperature response for LITT of prostate for spherical geometry as a function of time and radius showing radius of vaporization (T>100°C), radius of coagulation (T>60°C), and damage radius (Ω>0.53).

TABLE 5. Calculated Time to Create 10, 15, or 20 mm Damage Diameters (Ø) in Vivo

Prostate Laser power [W]	Perfusion: 0.1 ml/(g·min) Time to reach damage diameter [min:s]			Perfusion: 0.2 ml/(g·min) Time to reach damage diameter [min:s]		
	Ø = 10 mm	Ø = 15 mm	Ø = 20 mm	Ø = 10 mm	Ø = 15 mm	Ø = 20 mm
3	3:11	7:49	26:15	3:51	12:27	—
4	2:02	4:46	11:30	2:14	5:49	22:27
5	1:30	3:32	7:51	1:36	4:00	10:34
6	1:13	2:51	6:08	1:16	3:07	7:26
7	1:01	2:25	5:07	1:04	2:36	5:54
8	0:53	2:07	4:27	0:55	2:15	4:59
9	0:47	1:53	3:58	0:48	1:59	4:21
10	0:42	1:43	3:35	0:43	1:48	3:54
Liver Laser power [W]	**Perfusion: 0.5 ml/(g·min) Time to reach damage diameter [min:s]**			**Perfusion: 1.0 ml/(g·min) Time to reach damage diameter [min:s]**		
	Ø = 10 mm	Ø = 15 mm	Ø = 20 mm	Ø = 10 mm	Ø = 15 mm	Ø = 20 mm
3	3:01	—	—	—	—	—
4	1:51	8:02	—	2:31	—	—
5	1:23	4:46	49:50	1:41	11:13	—
6	1:08	3:36	12:56	1:19	5:29	—
7	0:58	2:58	8:29	1:05	3:58	—
8	0:51	2:34	6:39	0:57	3:14	14:48
9	0:46	2:18	5:37	0:50	2:46	9:21
10	0:42	2:05	4:56	0:46	2:27	7:15
Kidney Laser power [W]	**Perfusion: 2.0 ml/(g·min) Time to reach damage diameter [min:s]**			**Perfusion: 4.0 ml/(g·min) Time to reach damage diameter [min:s]**		
	Ø = 10 mm	Ø = 15 mm	Ø = 20 mm	Ø = 10 mm	Ø = 15 mm	Ø = 20 mm
3	—	—	—	—	—	—
4	—	—	—	—	—	—
5	—	—	—	—	—	—
6	2:50	—	—	—	—	—
7	1:47	—	—	—	—	—
8	1:22	8:29	—	—	—	—
9	1:08	5:09	—	—	—	—
10	0:59	3:55	—	1:32	—	—

(liver: ≥2.5 W, 10 min.) should be analyzed with precaution.

Simulations

Comparing the simulations with experimental coagulation diameters without carbonization revealed good agreement with an average deviation of ~1 mm or 10%, which was within the margin of error introduced by the measurements (Tables 3, 4). The measured lesion sizes tended to be slightly larger than the calculated coagulation diameters predicted, but they were within the damage diameters. This should be expected since the coagulation diameter only describes the acute tissue denaturation while neglecting the accumulation of more subtle damage at lower temperatures. It generally underestimates the extent of damage. Although the damage diameter provides an integral description of tissue damage, it may not be easy to measure. The loss of vitality from low level laser exposure over an extended duration may take days to express itself (hyperthermia). In conclusion, the laser–tissue interaction simulated by model calculation was sufficiently realistic to predict experimental in vitro results for coagulation.

Simulations of in vitro experiments in different tissues have shown that the induced coagulation diameters reached almost the same values in prostate and kidney, although the penetration depth, the absorption, and the scattering coefficients were significantly different. For interstitial laser treatment over an extended duration, temperatures far from the applicator are mainly determined by heat conduction, whereas light distribution plays a minor role. Subsequently, uncertainties in the determination of the optical tissue parameters, which were in the range of ±20%, did not influence the calculated coagulation diameters. The optical tissue properties, how-

ever, define the temperature distribution near the applicator and thus the risk of carbonization.

Since the model was in reasonably good agreement with the experimental data in vitro, it was interesting to assess its extension toward predicting the effects of in vivo treatment of patients. To obtain the same damage radius for prostate in vivo as in vitro, the model predicted significantly shorter exposure durations. This was no surprise since the necessary temperature rise is less dramatic when starting from body temperature than from room temperature in vitro. A small damage zone of 10 mm diameter should be easily reached in 2–3 min. with low laser powers of 3–4 W. Larger damage zones of 20 mm diameter would require slightly higher laser powers of 4–5 W to finish treatment in a reasonable time of 10 min. In contradistinction, kidney tissue with its high perfusion rate should require significantly higher laser powers to obtain even damage zones of 10 mm in diameter. The extension of the model toward in vivo irradiation simulations showed that blood perfusion plays an important role in predicting lesion sizes.

In conclusion, simulations and in vitro experiments with laser-induced thermotherapy suggest that a low power diode laser at 850 nm can be recommended to treat prostate and kidney tissue effectively in a reasonable amount of time. The treatment of kidney may benefit from a higher power diode laser because of its high perfusion rate. Due to the small penetration depth of 850 nm radiation in liver and the associated high risk of carbonization, diode laser-based LITT may not be recommended for use in liver tissue.

When comparing different tissues, one should note that the coagulation diameter depends on the individual tissue structure and protein composition. Different types of tissue are thus expected to have different coagulation thresholds. The model could be improved by using tissue specific constants A and E in the Arrhenius function in equation (1).

With the transition of tissue from coagulation to carbonization, the absorption coefficient increases drastically. Energy is no longer delivered to the tissue by photon diffusion but by heat conduction only. Coagulation diameters may be hard to predict in the presence of carbonization as demonstrated by the only two measured values (prostate: 4 W, 15 min; liver: 3 W 10 min), which deviated significantly from the simulations. Side effects, namely damage to the delivery system, may make carbonization an unfavorable and dangerous treatment modality. To limit the risk of carbonization, it is desirable to reduce the strong temperature rise at the applicator surface. Enlarging the applicator/catheter surface or cooling the catheter are alternatives that will be investigated in the future.

ACKNOWLEDGMENTS

The authors thank M. Lesiecki and G. Watson for many encouraging discussions and good suggestions. The contribution of Candela Laser Corporation, which made the diode laser system available and sponsored the study through an internal grant, is greatly appreciated.

REFERENCES

1. Muschter R, Hofstetter A, Hessel S, Keiditsch E, Rothenberger K-H, Scheede P, Frank F. Hi-tech of the prostate: Interstitial laser coagulation of benign prostatic hypertrophy. SPIE 1992; 1643:25–34.
2. Muschter R, Hofstetter A. "Thermische" Therapie der benignen Prostatahyperplasie, Münch Med Wschr 1992; 134:630–634.
3. Müller G, Wolf J, Fobbe F, Böse-Landgraf J, Germer C, Beuthan J, Roggan A. Interstitial laser hyperthermia: A new method to treat tumors. In: Spinelli P, Dal Fante M, Marchesini M, eds. "Photodynamic Therapy, and Biomedical Laser." New York: Excerpta Medica, 1992, pp 406–414.
4. Watson GM. Heat treatment of severe, symptomatic prostatic outflow obstruction. World J Urol 1991; 7–11.
5. Fan M, Ascher, PW Schröttinger O, Ebner F, Germann RH, Kleinert R. Interstitial 1.06 Nd:YAG laser thermotherapy for brain tumors under real time monitoring of MRI: Experimental study and phase I clinical trial. J Clin Laser Med Surg 1992; 10:355–361.
6. Jaques SL, Rastegar S, Motamedi M, Thomson SL, Schwatz J, Torres J, Mannonen I. Liver photocoagulation with diode laser (805 nm) vs. Nd:YAG laser (1064 nm). SPIE 1992; 1646:107–117.
7. Blackwell KE, Castro DJ, Saxton RE, Nyerges A, Calcaterre TC, Schiller, Grant V, Soudant J, Hirschowitz S, Hawkins R, Duckwiler G, Lufkin RB, Ward PH. MRI and ultrasound guided interstitial Nd:YAG laser therapy for pallitive treatment of advanced head and neck tumors: Clinical experience. J Clin Laser Med Surg 1993; 11:7–14.
8. Henrique Jr. FC, Moritz AR. Studies of thermal injury I,II,III. Am J Pathol 1947; 23:531–549, 695–720, 915–942.
9. Philipp C, Shaltout J, Zgoda F, Berlien H-P. Zur Problematik von Temperaturmessungen mit Thermoelementen während Laserbestrahlung in streuenden Medien. Lasermedizin 1992; 8:188–195.
10. Romeis, Benno. In: Bock P, ed. "Mikroskopische Technik." München: Urban & Schwarzenbeck, 1989.
11. Roggan A, Minet O, Schröder C, Müller G. Measurements of optical tissue properties using integrating

sphere technique. SPIE Institute on Medical Optical Tomographie, 1993; IS11.
12. Peters VG, Wyman DR, Patterson, Frank GI. Optical properties of normal and diseased human breast tissues in the visible and near infrared. Phys Med Biol 1990; 35:1317–1334.
13. Star MW, Marijnissen JPA, van Gemert MJC. Light dosimetry in optical phantoms and in tissues: 1.Multiple flux and transport theory. Phys Med Biol 1988; 33:437–454.
14. Takata AN, Zaneveld L, Richter W. Laser-induced thermal damage in skin. USAF School Aerospace Med., Brooks AFB, TX, Rep.SAM-TR-77-38, 1977.
15. Welch AJ. The thermal response of laser irradiated tissue. IEEE J Qant Electron 1984; QE-20:1471–1481.
16. Roggan A, Müller G. Computer simulations for the irradiation planning of LITT. Med Tech 1993; 4:18–24.
17. Shitzer A: General analysis of the bioheat equation. In: Shitzer A, Eberhard RC, eds. "Heat Transfer in Medicine and Biology," vol. 1. New York: Plenum Press, 1985.
18. Schuh H. Differenzverfahren zum Berechnen von Temperatur-Ausgleichsvorgängen bei eindimensionaler Wärmeströmung in einfachen und zusammengesetzten Körpern, VDI Forschungsheft Ausgabe B, Band 23, VDI Verlag Düsseldorf 1957; 459.
19. Schmidt RF, Thews G, eds. "Physiologie des Menschen." Heidelberg: Springer, 1983.
20. Takata AN. Development of criterion for skin burns. Aerospace Med. 1974; 45:634–637.
21. Beuthan J, Weber A, Minet O, Hagemann R, Roggan A, Schmitt I, Müller G, Germer CT, Albrecht D, Bocher T. Investigations concerning the determination of NADH-Concentration using optical biopsy. Lasermedizin 1994; 10:57–63.